1D core–shell magnetoelectric nanocomposites by template-assisted liquid phase deposition

Amin Yourdkhani[1], Daniela Caruntu[2] , Melvin Vopson[3], and Gabriel Caruntu[2,4]*

[1]Materials Engineering Department, Tarbiat Modares University, Tehran, Iran
[2]Department of Chemistry and Biochemistry, Central Michigan University 1200, S. Franklin St. Mount Pleasant, MI 48858 USA
[3]Department of Earth and Environmental Sciences, School of Earth & Environmental Sciences, University of Portsmouth, Burnaby Building Burnaby Road Portsmouth PO1 3QL, UK
[4]The Science of Advanced Materials (SAM) Program; Central Michigan University 1200, S. Franklin St. Mount Pleasant, MI 48858 USA; E-mail: carun1g@cmich.edu

We demonstrate here that 1D magnetoelectric core-shell nano-architectures can be rationally designed by a two-step procedure using the template-assisted liquid phase deposition (LPD) method. Highly crystalline $BaTiO_3$ nanotubes with an average diameter of 20 nm and controllable wall thickness were synthesized by immersing alumina templates into a treatment solution containing the perovskite precursors at temperatures as low as 40 ^oC. By a similar procedure the resulting ferroelectric nanotubes immobilized within the channels of the anodic aluminum oxide (AAO) membranes have been subsequently filled with a spinel ferrite phase, with the chemical composition $Zn_{1.5}Fe_{1.5}O_4$ yielding spinel-perovskite 1D core-shell magnetoelectric architectures. The resulting core-shell tubular nanocomposites have been synthesized and characterized structurally, morphologically and compositionally and their ferroelectric, magnetic and magnetoelectric properties have been investigated both qualitatively and quantitatively. A change from a superparamagnetic to a ferrimagnetic behavior was observed in the pristine spinel ferrite nanotubes when they have been incorporated into the spinel-perovskite core-shell nanocomposites, which clearly indicates the existence of a magnetoelectric coupling between the two ferroic phases. Moreover, the measured magnetoelectric coupling coefficient was α=1.08 V/cm·Oe, value which is superior to the values reported for similar thin film and tubular spinel ferrite magnetoelectric nanocomposites, thereby making indicating a strong strain-mediated coupling between the ferroelectric and magnetostrictive phase in the 1D core-shell nanocomposites and making these materials suitable for implementation into various functional devices.

1. INTRODUCTION

The coexistence of ferromagnetic, ferroelectric and ferroelastic order parameters is a characteristic feature of an important class of functional materials, known as magnetoelectric (ME) multiferroics. In such materials an electric current can be induced upon application of an external magnetic field (the direct ME effect) and vice-versa (the converse ME effect). In terms of the material constituents, multiferroics are generally divided into two categories: single phase and composites. Unfortunately, the ME coupling in single phase multiferroics is not as strong as the one exhibited by magnetoelectric composites. Moreover, this generally occurs at temperatures well below the room temperature, which drastically limits the use of single phase multiferroics in practical applications. When a ME composite material is subjected to the action of a magnetic or electric field, the ferroelectric/magnetic phase, which possesses electrostrictive or magnetostrictive properties, will respond to the external stimulus by changing its physical dimensions. This will induce a stress in the ferroelectric/magnetic phase, which is transferred across the shared interface to the other phase, eventually leading to a change of its ferroic properties. Since the interphase boundary between ferroic phases plays a key role in the ME coupling, there is an increasing technological interest in designing magnetoelectric nanocomposites with a high interfacial contact between the constituent magnetic and electrostrictive phases. Magnetoelectric hybrid nanocomposites consisting of a ferromagnetic and a ferroelectric phase can be designed generally in three different geometries: particulate nanocomposite films with magnetic particles embedded in a ferroelectric matrix (also referred to 0-3 nanocomposites), vertical heterostructures with one-phase nanopillars (1-3), horizontal heterostructures with alternating ferroelectric and magnetic layers (2-2) and one dimensional (1-core-shell structures (nanotubes and nanocables) having the magnetic and ferroelectric materials as core and shell, respectively, (1-1).[1-3] It has been predicted that 1D ME core-shell nanocomposites exhibit a stronger ME coupling compared to the other types of nanocomposites as a result of the higher interfacial contact area between the constituting phases and the absence of the clamping effect exerted by the substrate as commonly observed in bilayered ME nanostructures.[4] From this point of view, 1D ME core-shell nanocomposites are promising materials for the miniaturization of ME devices such as ME self-sensing cantilever actuators.[5] Several methods have been proposed to fabricate 1D ME core-shell nanocomposites consisting of magnetostrictive spinel ferrites and ferroelectric perovskite titanates. These approaches are mainly based on successive sol-gel processing steps using anodic aluminum oxide (AAO) membranes to confine the magnetic oxide core within the ferroelectric oxide shell[6], electrodeposition of ferromagnetic transition metals into the free space of ferroelectric oxide nanotubes embedded into a AAO membrane[7], and electrospinnig in combination with a sol-gel method.[8] Liquid phase deposition (LPD) is a soft chemical technique based on the slow hydrolysis of metal-fluoro complex species at temperatures below 60°C. The hydrolysis occurs via an equilibrium reaction whereby the fluoride ions from the inner coordination sphere of the metal are gradually replaced by OH^- ions and/or water molecules yielding mixtures of metal hydroxydes/oxyhydroxides. These reaction intermediates can be converted into the desired oxide phases upon a heat treatment at temperatures typically between 400 and 800 ^oC. LPD is simple, environmentlally friendly and does not require expensive vacuum equipment. Also, these reactions can be performed at low temperatures and the method allows surfaces with complex spatial geometries to be coated uniformly, thereby making the method attractive for the deposition of the high quality thin films of the functional ceramic oxides. In the absence of a fluorine scavenger, the hydrolysis reaction of metal fluoro-complexes in supersaturated solutions is slow at room temperature and occurs with reaching an equilibrium (reaction 1). Upon the addition of boric acid to the treatment solution, the fluoride ions are progressively scavenged from the solution yielding a stable water soluble complex of $[BF_4]^-$ ion (reaction 2).

$$MF_n^{(n-2m)-} + mH_2O \rightleftharpoons 1\,MO_m + nF^- + 2mH^+ \quad (1)$$

$$H_3BO_3 + 4HF \rightleftharpoons BF_4^- + H_3O^+ + 2H_2O \quad (2)$$

The liquid phase deposition method was initially proposed by Deki *et. al*. for the fabrication of silica thin films being subsequently extended to other ceramic oxides such as TiO_2[9], SiO_2[10], ZrO_2[11], SnO_2[12], Fe_2O_3[13]and NiO.[14] Recently, the liquid phase deposition method has been extended to complex ceramic metal oxides such as spinel ferrites AFe_2O_4 (A=Co, Ni and Zn)[15,16], perovskites ABO_3 (A= Ba, Sr and Pb, B=Ti and Zr)[17,18], magnetoplumbite hexagonal ferrite and bilayered of perovskite/spinel ferrites composite structures, respectively.[19] Due to the ability of the LPD technique to coat surfaces with complex spatial geometry, this method has been also extended to the fabrication of patterned nano-objects and 1D nanostructures. Based on replica lithography, Deki and coworkers fabricated highly ordered vertically aligned iron oxide nanopillars using the LPD technique.[20] Our group reported recently on the fabrication of uniform spinel ferrite $M_xFe_{3-x}O_4$ (M=Ni, Co, Zn)[21] and ABO_3 (A=Ba and Sr)[22] nanotube arrays with diameters of 200 nm by using the LPD route combined with a template-assisted approach. As the use of the conventional measurement set-up for bulk magnetoelectric composites is very limited to nanostructures due to difficulties in the separation of the ME signal and noise, recently complementary experimental techniques, such as Raman spectroscopy and scanning probe microscope (SPM) have been introduced to magnetoelectric characterization of bilayered nanocomposites.[23,24]

The direct strain mediated magnetoelectric effect has been qualitatively demonstrated in bilayered nanocomposites by tracking the changes in the wavenumbers of the lattice dynamic vibrations corresponding to the ferroelectric phase in the presence of a magnetic field.[19,25] Although magnetic field-assisted Raman spectroscopy is not enabled for the nanoscale magnetoelectric characterization of nanocomposites such as core-shell nanotubes and nanocables due to the diffraction limit of the visible light, piezoelectric force microscopy (PFM) has been introduced as a robust tool to characterize the ferroelectric and piezoelectric materials at the nanoscale by imaging the ferroelectric domains and measuring the local piezoelectric properties.[26-29] Recently, a novel PFM–based technique has been used by our research group to evaluate the magnetoelectric properties of the multiferroic nanocomposites.[30] This is based on the ability of the PFM method to probe nanoscale objects due to the nanometer size and the geometry of the conductive tip, thereby enabling the measurement of the piezoelectric properties of a single 1D multiferroic nanocomposite in the presence of an in-plane *dc* magnetic field and the measurement of the direct magnetoelectric coefficient. In this paper we report on the synthesis and characterization of the 1D ferroelectric $BaTiO_3$ nanostructures and their subsequent use to design tubular core-shell spinel-perovskite magnetoelectric nanocomposites by using the template-assisted liquid phase deposition (LPD) method. Due to the assembled nature of such composite structures, the work inherently requires the presence of several successive steps, including the synthesis of pristine spinel and ferrite nanotubular structures, the filling of the nanotubes of ferroelectric phase with the ferrite magnetic one, the structural, morphological characterization (local and bulk) of the individual ferroic phases, and the measurement of their ferroic properties, as well as of the measurement of the strain-mediated magnetoelectric coupling effect in ceramic hybrid 1D nanostructures.

2. EXPERIMENTAL PROCEDURE

2.1. Synthesis of ferroic and multiferroic metal oxide nanotube arrays

Coaxial magnetoelectric nanotubular structures consisting of a ferrite core and a ferroelectric perovskite phase as the shell have been fabricated by a two-step template-assisted procedure represented schematically in Fig. 1. First, ferroelectric $BaTiO_3$ nanotubes were synthesized within the pores of alumina membranes using treatment solutions obtained by mixing a 0.025 M aqueous solution of $(NH_4)_2TiF_6$ (0.025 M) with a 0.075 M solution of H_3BO_3 and a 0.025 M solution of $BaIJNO_3)_2$, respectively. All solutions were prepared by Alfa Aesar reagent grade purity chemicals dissolved in deionized (DI) water (18 MΩ) obtained from a Barnstead Nanopure water purification system.

The commercial anodized aluminum oxide (AAO) membranes were obtained from Whatman and had a thickness of 60 μm and an average pore diameter of 200 nm. Prior to de-position, the membranes were masked on one side using Scotch tape and then immersed in the treatment solution in a vertical position. During the deposition process, the solution was maintained at 40 °C to increase the rate of hydrolysis of the cationic species present in solution and promote the precipitation of amorphous oxyhydroxides inside the pores of the alumina template. At the end of the deposition process, the AAO templates were removed from the solution, rinsed carefully with deionized (DI) water and dried at room temperature for 3 hours. It is worth noting that the formation of nanotubes within the pores of the membranes is accompanied by the deposition of metal hydroxide/oxyhydroxide films on both sides of the AAO membranes. The formation of the films can be avoided by masking one side of the membrane with Scotch tape whereas films formed on the other side can be easily removed by mechanical polishing while keeping the nanotubes within the channels of the template. Since the resulting nanotubes are amorphous, a subsequent heat treatment at 750 °C in air was necessary to promote dihydroxylation and dehydration reactions and convert the intermediates into the desired $BaTiO_3$ nanotubes. The fabrication of 1D coaxial magnetoelectric structures involves the filling of the perovskite nanotubes with a magnetic spinel ferrite phase. As we demonstrated previously, the liquid phase deposition method is very versatile for the fabrication of 1D and 2D transition metal ferrite nanostructures with variable chemical composition and tunable magnetic properties.[16,19,21] To illustrate the viability of the proposed synthetic approach, we chose zinc ferrite as the magnetic phase for the fabrication of the 1D core–shell multiferroic nanocomposites. To this end, AAO membranes containing BTO nanotubes immobilized within their channels were immersed into a treatment solution obtained by dissolving 0.25 g of FeOOH dissolved in 50 ml of a 1 M NH_4·HF and mixing the resulting solution with a 2.22 M solution of $ZnIJNO_3)_2$ and 40 ml of 0.5 M boric acid solution, respectively. The complete filling of the perovskite nanotubes with the spinel ferrite phase was achieved by immersing the AAO templates into the treatment solution for 2 hours at 45 °C. A progressive change in the color of the AAO templates from white to brown was observed during the deposition process, thereby indicating the filling of the perovskite nanotubes with the amorphous zinc ferrite oxyhydroxide. The resultant coaxial 1D magneto-electric nanostructures have been characterized either in the form of free standing nanotubes or confined within the pores of the AAO templates. Free standing $BaTiO_3$ nanotubes coaxial ferrite-perovskite nanostructures were obtained by dissolving the AAO template in a 6 M sodium hydroxide solution for 30 min, followed by washing the 1D nanostructures followed by centrifugation and drying at 100 °C for 6 hours.

2.2. Characterization

(a) Transmission electron microscopy (TEM) and elemental analysis by energy-dispersive X-ray spectroscopy (EDX) and inductive coupling plasma (ICP) spectroscopy using a Varian FT220S flame absorption spectrometer. For chemical composition analysis, glass substrates were immersed vertically in the treatment solution and the resulted films were heat treated to induce crystallization of the oxide phases similar to the case of nanotubes and core–shell 1D nanostructures. For ICP experiments, these films were dissolved in 1 M HCl solutions under sonication for 20 minutes and the resulting solutions were used to determine the chemical composition of the perovskite and spinel phases, respectively.

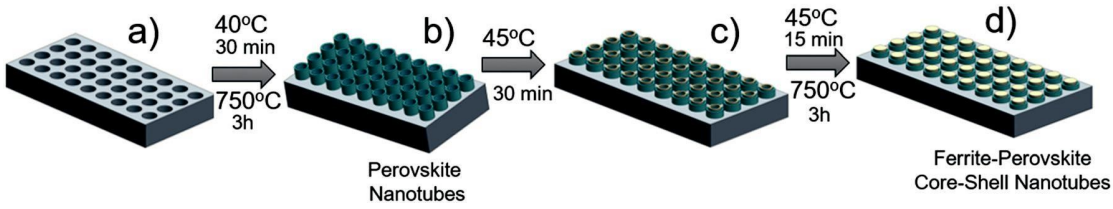

Fig. 1 Schematic representation of the two-step template-assisted procedure for the fabrication of 1D core–shell ferrite-perovskite magnetoelec-tric nanocomposites by the liquid phase deposition method: (a) the AAO template; (b) perovskite nanotube arrays confined within the channels of the AAO template, perovskite nanotubes partially (c) and completely (d) filled with a transition metal ferrite.

The morphology, phase purity and crystallinity of the $BaTiO_3$ nanoparticles were investigated by transmission electron microscopy (TEM), HRTEM, EDX and SAED with a JEOL 2200FS microscope with a resolution of 0.19 nm at a bias voltage of 200 kV and a FE-SEM (JEOL 7500F). For electron microscopy experiments, several drops of solution containing metal oxide nanotubes/ coaxial spinel-perovskite ME nanocomposites were cast under ambient conditions onto carbon-coated copper TEM grids.

(b) Powder X-ray diffraction. The phase purity and the crystal structure of the nanomaterials were studied by powder X-ray diffraction (XRD) with a Panalytical X'Pert system using monochromatic Cu Kα radiation (λ = 1.54056 Å at 40 kV and 40 mA). Diffraction data were collected at room temperature by step scanning in the range $15° \leq 2\theta \leq 75°$ with a step size of 0.02° and a time per step of 10 s. The collected data were analyzed using the X'Pert High score software. The size of the crystallites was determined by the analysis of the three most intense peaks in the corresponding XRD patterns by the Scherrer method using polycrystalline silicon as a standard.

(c) Raman spectroscopy. Raman spectra were recorded with a Horiba Jobin Yvon Xplora Raman spectrometer using a 100× microscope objective and a 532 nm excitation of an Nd/YAG laser with a maximum power of 25 mW. The measurements were performed with a 10 μm pinhole and a spectral resolution of 1 cm^{-1}. The laser spot size was 2 μm and the collected data were analyzed with Labview 6 software provided by Horiba to precisely locate the Raman bands.

(d) Scanning probe microscopy. The polarization switch-ing, local ferroelectric and dielectric response of nanotubular materials were studied at room temperature with an Asylum Research (Oxford Instruments) MFP-3D atomic force microscope using a platinum/titanium coated cantilever (AC240TM, nominal spring constant 2 N m^{-1}, resonance frequency 70 kHz). The PFM measurements were performed on nanostructures dispersed onto an ITO glass substrate by applying a high-frequency modulating voltage to the tip. The magneto- electric coupling in the perovskite-spinel ferrite 1D nano-composites was investigated by piezoresponse force micros-copy in the presence of an in-plane magnetic field generated by a variable field (VFM2) module, which can generate static magnetic fields up to ±800 Oe with a 1 Oe resolution.

3. RESULTS AND DISCUSSION

The phase analysis and structural characteristics of the nano-tubular oxide structures and coaxial nanostructures were investigated by powder X-ray diffraction. The chemical composition of the perovskite nanotubes and ferrite core phase, determined by inductive coupled plasma spectroscopy indicated a molar Ba/Ti and Zn/Fe ratio of 1.01/0.99 and 1.5/1.5, corresponding to a formula of $BaTiO_3$ and $Zn_{1.5}Fe_{1.5}O_4$, respectively. As seen in Fig. 2, the $BaTiO_3$ nanotubes obtained during the first deposition step are single phase, without traces of $BaCO_3$ or anatase or rutile titania and possess a high crystallinity after a heat-treatment at 750 °C. Since no peaks characteristic to the tetragonal crystal structure, such as the {002}, {102} and {112} reflections were observed, the XRD pattern of the $BaTiO_3$ nanotubes has been indexed to the cubic structure (space group Pm3m). The lattice parameter refined with the CELREF software was found to be a = 4.029(3) Å.

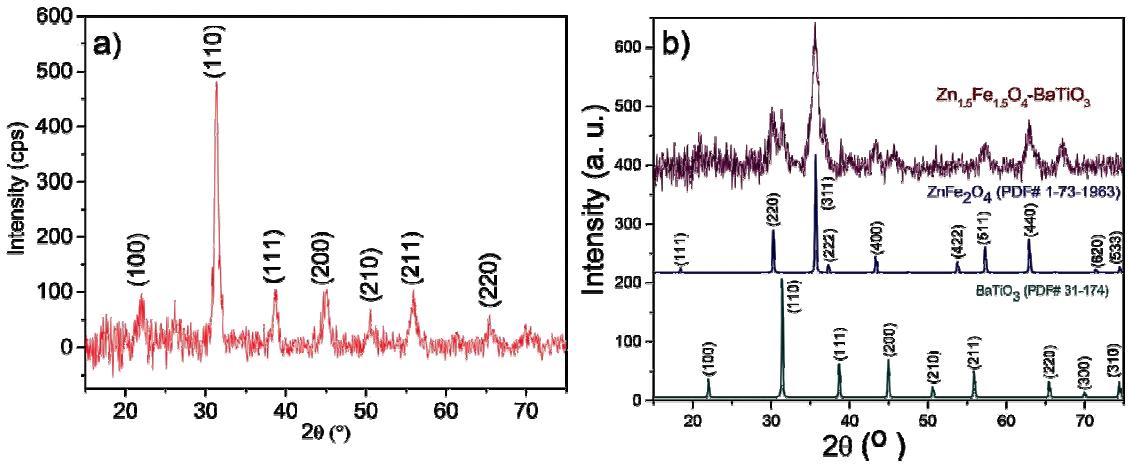

Fig. 2 X-Ray diffraction patterns of $BaTiO_3$ nanotubes (a) and $Zn_{1.5}Fe_{1.5}O_4$–$BaTiO_3$ core–shell magnetoelectric nanostructures (b) obtained by the template-assisted liquid phase deposition method.

As seen in Fig. 2b in the XRD pattern of the coaxial nanostructures a spinel ferrite phase (PDF No. 1-73-1963) and $BaTiO_3$ can be clearly identified, thereby confirming the formation of spinel-perovskite nano-composites. Both compounds are well crystallized after the heat treatment at 750 °C and do not contain secondary phases. The refined lattice parameter of the $Zn_{1.5}Fe_{1.5}O_4$ phase forming the core of the coaxial spinel-perovskite magnetoelectric structure is a = 8.32(8) Å, which is comparable to that of the bulk material (a = 8.35 Å).

It is worth mentioning that the apparent absence of the splitting of the (200) peak in the XRD pattern of $BaTiO_3$ nanotubular structures does not exclude the existence of an acentric ferroelectric phase since the reflections characteristic to the non-centrosymmetric polymorph may be obscured by the broadening effect associated with the small size of the crystalline domains diffracting coherently the X-ray radiation. To elucidate the tetragonal distortion in the $BaTiO_3$ phase, the crystal structure of the perovskite nanotubes was investi-gated by Raman spectroscopy at room temperature. As seen in Fig. 3, the Raman spectrum of the $BaTiO_3$ nanotubes presents well-defined bands associated with the existence of a tetragonally-distorted crystal structure. It is well-known that the highly symmetrical environment of the Ti^{4+} ions in the cubic $BaTiO_3$ polymorph, with the Ti^{4+} ions located in the center of the corner-sharing TiO_6 octahedra, precludes the existence of electrical dipoles and a ferroelectric order along with the absence of Raman activity.

However, in tetragonal $BaTiO_3$ (space group P4mm), the off-center shift of the Ti^{+4} ions leads to the formation of electrical dipoles, thereby inducing an intrinsic lattice polariza-tion.[31] At the same time, the lowering of the symmetry from cubic to tetragonal will also induce a splitting of the four de-generate $3F_{1u} + F_{2u}$ modes into eight Raman active transverse (TO) and longitudinal (LO) phonons represented by $3[A_1(TO) + A_1(LO)] + B_1 + 4[E(TO) + E(LO)]$.[32] As seen in Fig. 3, the Raman spectrum of the $BaTiO_3$ nanotubes present bands located around 276, 301, 516 and 720 cm^{-1} which have been assigned to the $A_1(2TO)$, $E(3TO) + E(2LO) + B_1$, $E(4TO) + A_1(3TO)$ and $E(4LO) + A_1(3LO)$ Raman modes, associated with stretching and bending modes of tetragonal polymorph, which confirms the existence of local tetragonal distortions in the corresponding $BaTiO_3$ tubular nanostructures.

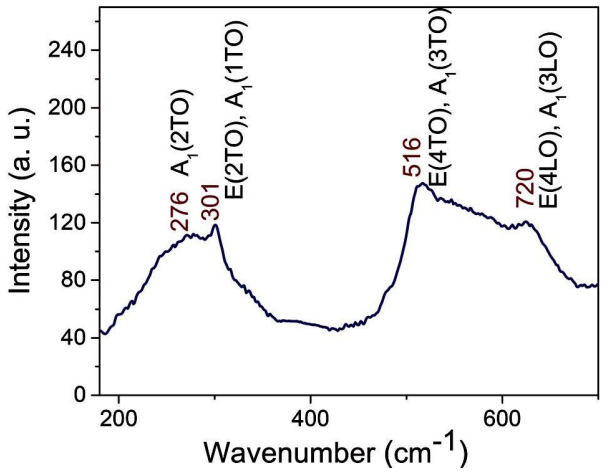

Fig. 3 Representative Raman spectrum of $BaTiO_3$ nanotubes obtained by the liquid phase deposition (LPD) model.

It is also worth noting that the bands at 301 and 720 cm^{-1}, which are generally considered the signature of the tetragonal structure, are well-defined and relatively strong in intensity, thereby confirming the acentric structure of the nanotubes. The small bump observed around 400 cm^{-1} has been conventionally ascribed to the presence of hexagonal $BaTiO_3$.[33] The FE-SEM images of the

$BaTiO_3$ nanotubular structures obtained by the LPD method and heat treated at 750 °C are shown in Fig. 4a–c. Fig. 4a shows $BaTiO_3$ nanotubes confined within the channels of the AAO template obtained by soaking the alumina membrane in the treatment solution for 30 minutes.

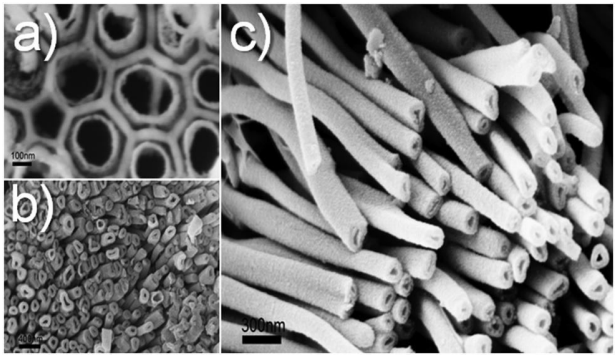

Fig. 4 FE-SEM images of $BaTiO_3$ nanotubular architectures: confined within the channels of anodized AAO templates (a), partially exposed (b) and free standing nanotubes (c).

The perovskite tubular nanostructures are relatively uni-form in size and possess an average diameter of 200 nm, which is comparable to the diameter of the channels of the template. It must be noticed that due to the relatively low pH of the treatment solution the AAO templates can be partially etched during the deposition of the perovskite nanotubes, which may lead to an increase of the diameter of the inner channels as previously reported in the literature.[34] However, our experimental results revealed that the pH of the treatment solution increased progressively from 3.9 to 4.5 during the deposition. As such, a less acidic medium will slow down the etching of the AAO template resulting in nanotubular structures with average diameter sizes very close to those of the pores of the parent AAO template. Fig. 4b shows $BaTiO_3$ nanotubes obtained after five hours of deposition and partially released from the alumina template by etching the sample with H_3PO_4 5% (weight) for 15 min. Fig. 4c shows a close-up of $BaTiO_3$ nanotubes obtained after removing completely the AAO template. Free standing nanotubes are high quality and possess open ends, smooth surfaces being free of defects such as cracks and holes. These characteristics make the template-assisted liquid phase deposition very attractive for the deposition of oxide nanotubes with various chemical composition. This is because, in addition to its low cost and simplicity the LPD method leads to the formation of defect-free nanotubes, unlike other template-assisted techniques, which yield nanotubular architectures with extended defects, such as cracks and holes as a result of the Rayleigh–Taylor in-stabilities[35] during the wetting process of the pore walls and the pyrolysis of the sol during the heat treatment. Addition-ally, in the conventional AAO template assisted sol–gel synthesis of metal oxides the degree of filling of the pores cannot be controlled, which renders to control the wall thickness and the physical properties of the nanotubes almost impossible. Unlike the sol–gel process, we demonstrated that, from a mechanistic point of view, metal oxides with variable architectural complexity (1D or 2D) are formed in the liquid phase deposition method via the attachment of fine particles initially formed in solution.[16]

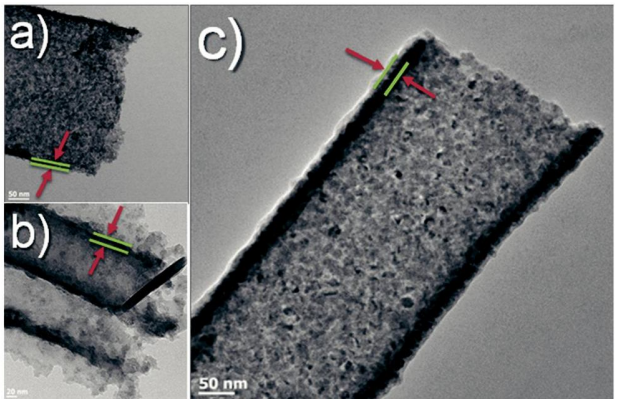

Fig. 5 TEM images of $BaTiO_3$ nanotubes with various wall thickness: 9 nm (a), 20 nm (b) and 32 nm (c). To vary the wall thickness, the deposition time increased from 0.5 to 3 and 5 h, respectively.

Fig. 5a–c show representative transmission electron microscopy (TEM) images of the $BaTiO_3$ nanotubes synthesized by soaking the AAO templates into the treatment solution for different periods of time. As seen in the TEM micro-graphs, the wall thickness of the $BaTiO_3$ nanotubes increased from 9 to 20 and 32 nm when the deposition time was varied from 0.5 to 3 and 5 h, respectively. Based upon the proposed mechanism, nanotubes form initially on the surface of the pores, process which is followed by the progressive deposition of the metal oxide towards the inner volume of the tem-plate's channels. This nucleation process will allow the control of the wall thickness of the nanotubes by simply varying the deposition time at a particular temperature.

The piezoelectric response of the nanotubes with three different thicknesses was measured by SSPFM and the corresponding piezo-amplitude butterfly loops of the nanotubes with wall thicknesses of 9, 20 and 32 nm are presented in Fig. 6.

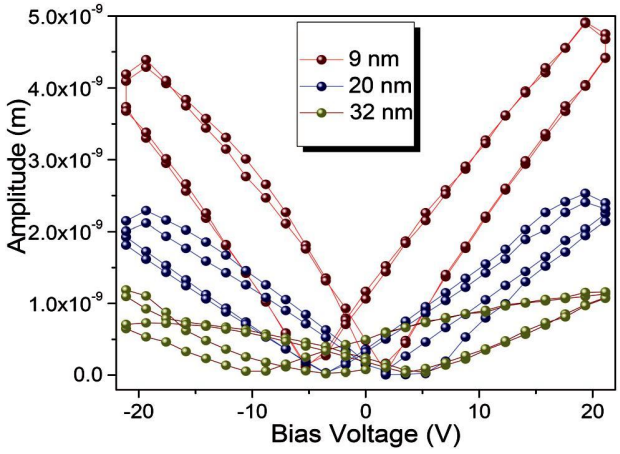

Fig. 6 Amplitude PFM butterfly loops of $BaTiO_3$ nanotubes with various wall thickness.

The corresponding piezoelectric response strongly depends on the wall thickness of the nanotubes via effects involving the surface tension and near-surface eigenstrain re-laxation.[36] Specifically, the surface tension induces radial and shear stresses in the cylindrical geometry of the nanotubes, thereby enhancing the polarization values and the ferroelectric phase transition temperature of the

nanotubes. Moreover, the longitudinal piezoelectric coefficient (d_{33}) of the ferroelectric nanotubes is directly proportional to the polarization values. The fitting of the linear portion of the amplitude signal lead to measured d_{33} values of 5.2, 11.4 and 22.2 pm V^{-1} for nanotubes having wall thicknesses of 9, 20 and 32 nm, respectively

For scanning probe microscopy measurements, the as-synthesized $BaTiO_3$ nanotubes were dispersed in DI-water and then drop cast on highly doped (100) silicon substrates. Fig. 7a shows the topography of two $BaTiO_3$ nanotubes attached together and Fig. 7b and c correspond to the piezoresponse (phase and amplitude) images of the nanotubes. The marked areas in the phase images were electrically polled by applying a 22 V DC voltage perpendicular to the axis of the nanotubes by placing the conductive tip in contact with the surface. The polled areas appear with a different contrast in the corresponding PFM images. The cross-sectional values of the line drawn in Fig. 7b have been plot-ted as a function of the line distance. The phase shift between the poled and non-poled areas is about 180°, value which strongly suggests that a sharp transition between polarization states occurred when the sample was subjected to an electric field higher than the local coercive field. Switching spectroscopy piezoelectric force microscopy (SSPFM) was used to evaluate the piezoelectric properties of an individual nanotube using a conductive tip as a top electrode in capaci-tor geometry while the highly doped Si substrate acted as the bottom electrode. Both the phase and amplitude piezoresponse signals were collected locally by applying a square-triangular voltage with amplitude of 22 V and a frequency of 400 mHz through the conductive tip.

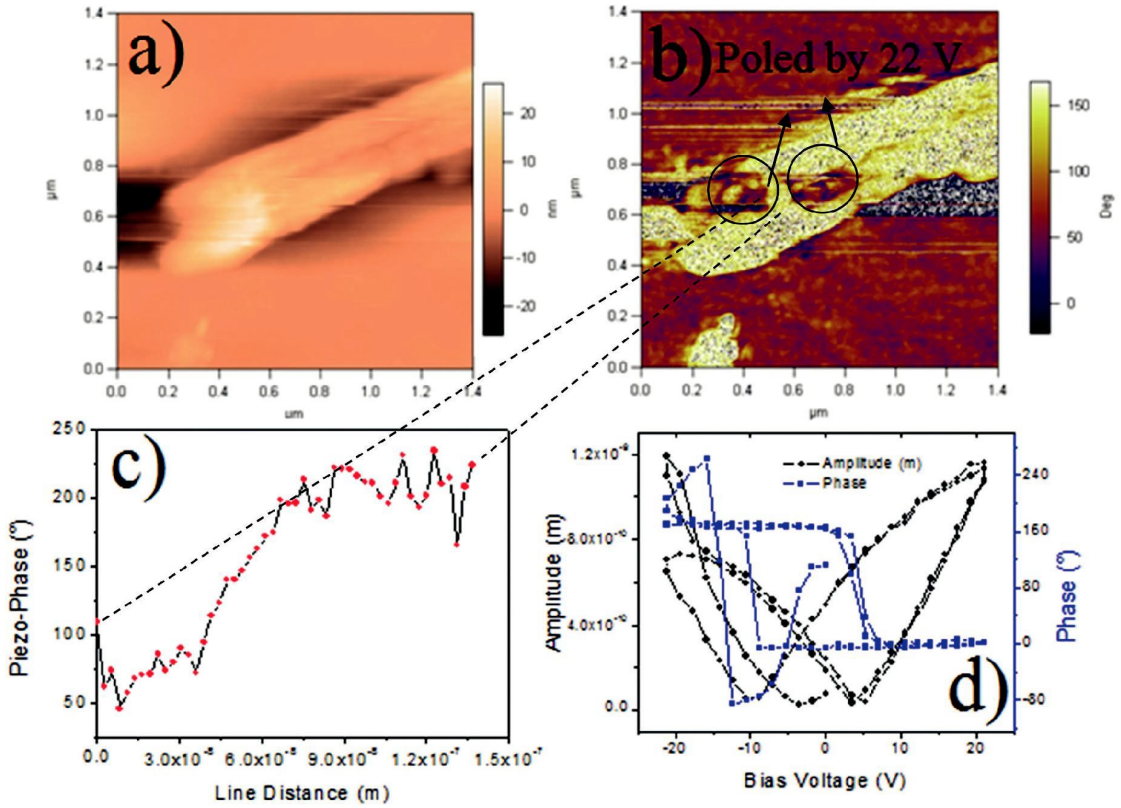

Fig. 7 a) AFM topography of $BaTiO_3$ nanotubes, b) Piezo-phase image c) line scan of the piezo-phase image on the drawn line on the piezo-phase image and d) piezo-amplitude and piezo-phase hysteresis loops versus applied voltage.

The piezoresponse of individual nanotubes as a function of the applied bias voltage is shown in Fig. 7d. The piezoelectric response shows a hysteretic behavior with a 180° switch of the orientation of the dielectric polarization when the ap-plied voltage was progressively varied from 22 to −22 V. Such a behavior is associated with the reversible switching of the dielectric polarization between two possible orientations (up-wards and downwards, respectively), which further confirms the ferroelectric behavior of the $BaTiO_3$ nanotubes. The coercive field necessary to change the orientation of the dipoles was about 6.8 V. The amplitude signal versus the bias dc-voltage displays a butterfly-type loop (Fig. 7d). The slight shift of the butterfly loop toward the positive bias voltage can be seemingly attributed to the presence of surface charges between the conductive tip and the surface.

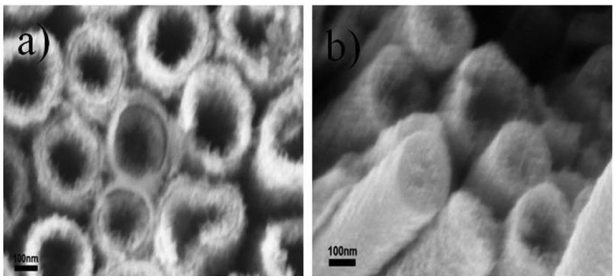

Fig. 8 FE-SEM images of $BaTiO_3$ nanotubes partially (a) and completely (b) filled with the zinc ferrite phase.

Fig. 8a and b show the FE-SEM images of the multiferroic nanocomposites consisting of magnetic (core) and ferroelectric (shell) phases of $Zn_{1.5}Fe_{1.5}O_4$ ferrite[21] and $BaTiO_3$, respectively.
The magnetic hysteresis loop of the $BaTiO_3/Zn_{1.5}Fe_{1.5}O_4$ nanocomposites is shown in Fig. 9a.

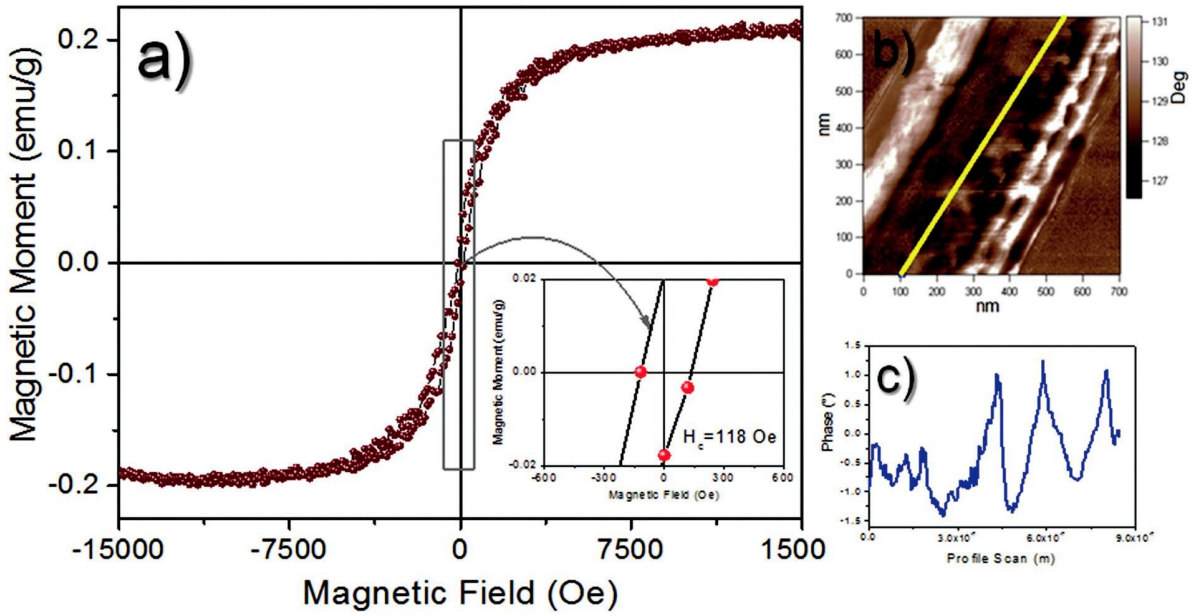

Fig. 9 a) Magnetic hysteresis loop, b) MFM image of the 1D multiferroic nanocomposites of $BaTiO_3$/Zn-ferrite and c) cross section profile of the magnetic phase for the line drawn on MFM image.

Compared to the super-paramagnetic behavior of pristine Zn-ferrite nanotubes, the $BaTiO_3/Zn_{1.5}Fe_{1.5}O_4$ core–shell 1D nanocomposites are ferro-magnetic. Such a drastic change in the magnetic properties of the ferrite phase with/without the ferroelectric phase can be tentatively ascribed to the increase of the total magnetic anisotropy of the ferrite when this is interfaced with $BaTiO_3$ in a composite geometry. The experimentally measured values of the coercive magnetic field (H_c) and magnetization saturation (M_s) of the $BaTiO_3/Zn_{1.5}Fe_{1.5}O_4$ nanocomposites were 118 Oe and 0.21 emu g^{-1}, respectively. Magnetic force microscopy was employed to image the magnetic domain configuration of the $BaTiO_3/Zn_{1.5}Fe_{1.5}O_4$ nanocomposites (Fig. 9b). As seen in the figure, strip-like regions with light and dark contrasts can be easily observed in the MFM image. These regions represent domains in which the magnetization is oriented either upwards (repulsive interaction) or down-wards (attractive interaction). Due to the cylindrical geometry of the 1D nanocomposites, some artifacts appeared at the edges whereby the magnetic tip cannot properly raster scan the surface of the sample. The changes in the magnetic phase corresponding to the cross-section line drawn in Fig. 9b have been plotted versus the line distance (Fig. 9c). The magnetic phase changes when the line passes across regions having different magnetic domain configurations of the magnetic phase. Recently, a novel technique based on the piezoelectric force microscopy technique has been developed by our research group for the evaluation of the stress-mediated ME properties of multiferroic nanocomposites. $BaTiO_3/Zn_{1.5}Fe_{1.5}O_4$ 1D nanocomposites dispersed in DI-water and were drop cast on a (001) Si substrate. The piezoelectric properties of the 1D core–shell nanocomposite were measured in the presence of a uniform in-plane dc magnetic field produced during the PFM measurements with a variable field module (VFM).

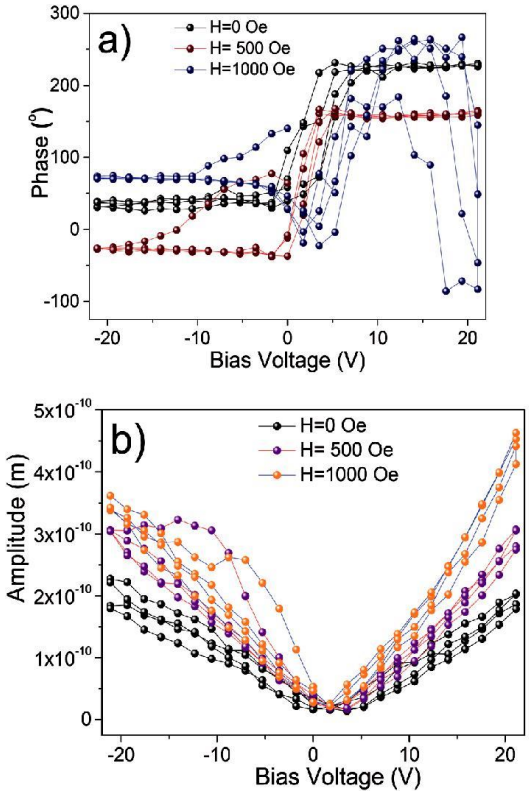

Fig. 10 Piezoelectric phase (a) and amplitude (b) hysteresis loops of the 1D core–shell magnetoelectric $BaTiO_3/Zn_{1.5}Fe_{1.5}O_4$ nanocomposites in the presence of a magnetic field.

Fig. 10 illustrates the loops of the phase and the amplitude versus the bias voltage for the 1D multiferroics nanocomposite of $BaTiO_3/Zn_{1.5}Fe_{1.5}O_4$ in a horizontal magnetic field. The difference between the maximum and mini-mum values of the piezo-phase when the bias voltage was swept from −22 to +22 V is about 180°, which indicates the existence of 180° ferroelectric domains in the $BaTiO_3$ nano-tubular architectures. Similar to the case of the parent $BaTiO_3$ nanotubes, the piezo-amplitude vs. voltage loops exhibit the well-known "butterfly-type" behavior which is characteristic to ferroelectric materials. As it can be seen in Fig. 10b, the slope of the piezo-amplitude signal increased when the magnetic field varied from 0 to 500 and 1000 Oe, respectively.
The piezoelectric coefficients (d_{33}) were calculated by fitting the linear portion of the butterfly loops and the corresponding values were 27.54, 47.04 and 81.72 pm V^{-1} for ap-plied magnetic fields of 0, 500 and 1000 Oe, respectively. This systematic variation in the piezoelectric coefficient of the sample originates from a strain-mediated ME coupling between the two ferroic phases of the nano composite material.[37]

3.1. Calculation of the direct magnetoelectric coefficient

The Gibbs free energy for a multiferroic system as a function of temperature, pressure, electric field and magnetic field is expressed by eqn (1).[38]

$$dG = Vdp - SdT - PdE - MdH \quad (1)$$

where V is the volume, p is the pressure, S is the entropy, P is the polarization, E is the electric field, M is the magnetization and H is the magnetic field. At a constant pressure and temperature eqn (1) can be simplified to eqn (2) as following:

$$dG = -PdE - MdH \quad (2)$$

By using the equality of cross derivatives, eqn (2) becomes:

$$\left(\frac{\partial P}{\partial H}\right)_E = \left(\frac{\partial M}{\partial E}\right)_H \quad (3)$$

The term above is known as magnetoelectric (ME) coefficient in which measuring the change in polarization by vary-ing the magnetic field is the direct magnetoelectric coefficient $\alpha_{direct} = \partial P/\partial H$, while measuring the change in magnetization by variation of the electric field is the indirect ME coefficient, coefficient $\alpha_{direct} = \partial M/\partial E$.
From the thermodynamics of ferroelectrics, the piezoelectric coefficient and polarization are related by following equation:[39]

$$d_{33} = 2\varepsilon_{33}QP \quad (4)$$

where Q is electrostrictive coefficient and ε_{33} is out of plane component of dielectric permittivity tensor. By replacing the $P = d_{33}/2Q\varepsilon_{33}$ in the direct ME coefficient equation, the following equation is obtained:

$$\alpha_{\text{direct}} = \left(\frac{\partial P}{\partial H}\right)_E = \frac{1}{2Q\varepsilon_{33}}\left(\frac{\partial d_{33}}{\partial H}\right)_E \quad (5)$$

By combining the $\sigma = - E/g_{33}$ (6) and $g^{33} = d_{33}/\varepsilon_{33}$ (7) with (5) where g_{33} is the piezoelectric coefficient, we obtain:[38]

$$\alpha_{\text{direct}} = -\sigma\left(\frac{\partial d_{33}}{\partial H}\right)_E \quad (8)$$

The direct ME coefficient in eqn (8) is proportional to the mechanical stress (σ). In the case of the $BaTiO_3$/Zn-ferrite nanocomposites, the mechanical stress is compressive (negative term) while the term $\partial d_{33}/\partial H$ is positive. The variation of d_{33} coefficient with the magnetic field for the $BaTiO_3$/ $Zn_{1.5}Fe_{1.5}O_4$ 1D nanocomposites is shown in Fig. 11, leading to a value of the direct ME coefficient calculated from eqn (5) has a value $\alpha_{\text{direct}} = 1.08$ V cm^{-1} Oe^{-1}.

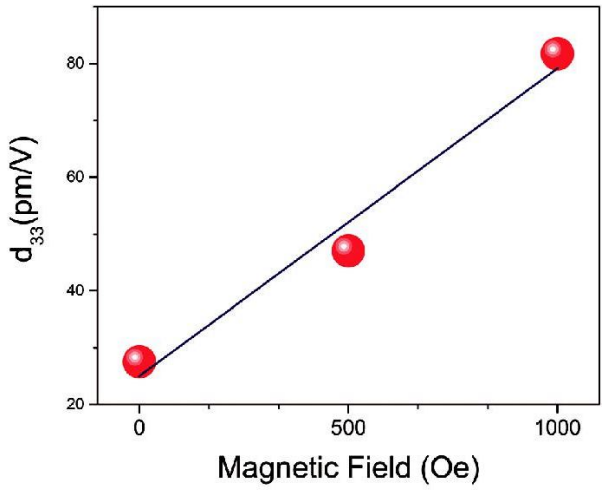

Fig. 11 Magnetic field-dependence of the longitudinal piezoelectric coefficient (d_{33}) of the 1D core–shell magnetoelectric spinel-perovskite nanocomposite.

A similar behavior also was observed in bilayered perovskite-spinel ferrite nanocomposites in which the mag-netic layers possessed both negative and positive magneto-striction coefficients and the variation of the piezoelectric coefficients is positive and negative, respectively.[37] We stress out here that positive/negative variation of the piezoelectric coefficient of the multiferroic nanocomposite in the presence of the magnetic field is dictated by negative/positive sign of the magnetostriction coefficient.

4. CONCLUSIONS

In summary, we demonstrate for the first time that the liquid phase deposition (LPD) method is a highly reliable yet less expensive route for the fabrication of magnetoelectric 1D core–shell nanocomposites. In the first step of the proposed experimental procedure highly pure, defect-free ferroelectric nanotubes with a dense microstructure were successfully fabricated within the channels of anodic aluminum oxide (AAO) templates by the controlled hydrolysis of stoichiometric amounts

of metal oxyfluoro complexes in the presence of boric acid used as a fluoride scavenger. The wall thickness of the perovskite nanotubes can be varied from 9 to 20 and 32 nm by increasing the deposition from 0.5 to 3 and 5 h, respectively. Piezoresponse force microscopy measurements (PFM) showed that the $BaTiO_3$ nanotubes exhibited a strong ferroelectric response room temperature, as indicated by both piezo-amplitude and piezo-phase components of the piezoelectric signal. The values of the longitudinal piezoelectric coefficient (d_{33}) of the $BaTiO_3$ nanotubes were found to de-crease from 22.2 to 11.4 and 5.2 pm V^{-1} when the wall thick-ness of the nanotubes increased from of 9, 20 and 32 nm. In the second step of the liquid phase deposition process a ferrite phase with the chemical composition $Zn_{1.5}Fe_{1.5}O_4$ was de-posited inside of the perovskite nanotubes, thereby yielding to 1D core–shell spinel ferrite-perovskite magnetoelectric nanostructures. The ferrite core exhibits a robust magnetic response at room temperature with a coercivity value H_c = 118 Oe. The investigation of the direct ME effect in these 1D nanocomposites by magnetic field-assisted piezoresponse force microscopy technique revealed the existence of a strong strain-mediated ME coupling effect with a value of the ME coefficient of 1.08 V cm^{-1} Oe^{-1}. The simplicity, low cost and versatility of the liquid-phase deposition process makes it attractive for the design of other metal oxide-based 1D nano-composites with tunable morphology and chemical composition for applications in sensing, catalysis, energy storage and electronics.

ACKNOWLEDGEMENTS

This work was supported by the National Science Foundation (NSF) through the CAREER grant No. 1434457 and the Central Michigan University through start-up funds.

REFERENCES

[1] C. W. Nan, M. I. Bichurin, S. Dong, D. Viehland and G. Srinivasan, J. Appl. Phys., 2008, 103, 031101.
[2] G. Srinivasan, in Annual Review of Materials Research, Vol 40, ed. D. R. Clarke, M. Ruhle and F. Zok, 2010, vol. 40, pp. 153–178.
[3] L. W. Martin, Y. H. Chu and R. Ramesh, Mater. Sci. Eng., R, 2010, 68, 89–133.
[4] G. Liu, C. W. Nan, Z. K. Xu and H. D. Chen, J. Phys. D: Appl. Phys., 2005, 38, 2321–2326.
[5] K. Prashanthi, M. Mandal, S. P. Duttagupta, R. Pinto and V. R. Palkar, Sens. Actuators, A, 2011, 166, 83–87.
[6] M. Liu, X. Li, H. Imrane, Y. Chen, T. Goodrich, Z. Cai, K. S. Ziemer, J. Y. Huang and N. X. Sun, Synthesis of ordered arrays of multiferroic NiFe2O4-PblJZr0.52Ti0.48)O3 core-shell nanowires, AIP, 2007.
[7] S. Xie, F. Ma, Y. Liu and J. Li, Nanoscale, 2011, 3, 3152–3158.
[8] K. Raidongia, A. Nag, A. Sundaresan and C. N. R. Rao, Multiferroic and magnetoelectric properties of core-shell CoFe2O4@BaTiO3 nanocomposites, AIP, 2010.
[9] S. Deki, Y. Aoi, O. Hiroi and A. Kajinami, Chem. Lett., 1996, 433–434, DOI: 10.1246/cl.1996.433.
[10] S. Deki, H. Y. Y. Ko, T. Fujita, K. Akamatsu, M. Mizuhata and A. Kajinami, Eur. Phys. J. D, 2001, 16, 325–328.
[11] K. Kuratani, M. Uemura, M. Mizuhata, A. Kajinami and S. Deki, J. Am. Ceram. Soc., 2005, 88, 2923–2927.
[12] Y. Saito, Y. Sekiguchi, M. Mizuhata and S. Deki, J. Ceram. Soc. Jpn., 2007, 115, 856–860.
[13] S. Deki, Y. Aoi, J. Okibe, H. Yanagimoto, A. Kajinami and M. Mizuhata, J. Mater. Chem., 1997, 7, 1769–1772.
[14] M.-K. Lee and C.-H. Fan, J. Electrochem. Soc., 2009, 156, D395–D399.
[15] G. Caruntu, A. Newell, D. Caruntu and C. J. O'Connor, Alloys Compd., 2007, 434, 637–640.
[16] G. Caruntu, G. G. Bush and C. J. O'Connor, J. Mater. Chem., 2004, 14, 2753–2759.
[17] M.-C. Hsu, Y.-M. Sun, I.-C. Leu and M.-H. Hon, Appl. Surf. Sci., 2007, 253, 7639–7644.
[18] M. K. Lee, H. C. Liao, K. W. Tung, C. M. Shih and T. H. Shih, J. Phys. D: Appl. Phys., 2002, 35, 61–64.
[19] A. Yourdkhani, A. K. Perez, C. K. Lin and G. Caruntu, Chem. Mater., 2010, 22, 6075–6084.

[20] S. Deki, S. Iizuka, A. Horie, M. Mizuhata and A. Kajinami, Mater. Chem., 2004, 14, 3127–3132.
[21] A. Yourdkhani and G. Caruntu, J. Mater. Chem., 2011, 21, 7145–7153.
[22] Y.-Y. Chen, B.-Y. Yu, J.-H. Wang, R. E. Cochran and J.-J. Shyue, Inorg. Chem., 2008, 48, 681–686.
[23] F. Zavaliche, H. Zheng, L. Mohaddes-Ardabili, S. Y. Yang, Q. Zhan, P. Shafer, E. Reilly, R. Chopdekar, Y. Jia, P. Wright, G. Schlom, Y. Suzuki and R. Ramesh, Nano Lett., 2005, 5, 1793–1796.
[24] L. Yan, Z. P. Xing, Z. G. Wang, T. Wang, G. Y. Lie, J. F. Li and D. Viehland, Appl. Phys. Lett., 2009, 94, 192902.
[25] Z. Li, Y. Wang, Y. H. Lin and C. W. Nan, Phys. Rev. B: Condens. Matter Mater. Phys., 2009, 79, 180406.
[26] Y. Kim, H. Han, W. Lee, S. Baik, D. Hesse and M. Alexe, Nano Lett., 2010, 10, 1266–1270.
[27] S. V. Kalinin, A. N. Morozovska, L. Q. Chen and B. J. Rodriguez, Rep. Prog. Phys., 2010, 73, 056502.
[28] A. N. Morozovska, E. A. Eliseev and S. V. Kalinin, J. Appl. Phys., 2007, 102, 074105.
[29] V. Anbusathaiah, S. Jesse, M. A. Arredondo, F. C. Kartawidjaja, O. S. Ovchinnikov, J. Wang, S. V. Kalinin and Nagarajan, Acta Mater., 2010, 58, 5316–5325.
[30] A. Yourdkhani, E. Garza, L. Zaldivar, L. Spinu and G. Caruntu, IEEE Trans. Magn., 2011, 47, 3939–3942.
[31] S. Adireddy, C. K. Lin, B. B. Cao, W. L. Zhou and G. Caruntu, Chem. Mater., 2010, 22, 1946–1948.
[32] U. D. Venkateswaran, V. M. Naik and R. Naik, Phys. Rev. B: Condens. Matter Mater. Phys., 1998, 58, 14256–14260.
[33] D. Erdem, Y. Shi, F. J. Heiligtag, A. C. Kandemir, E. Tervoort, L. M. Rupp and M. Niederberger, J. Mater. Chem. C, 2015, 3, 9833–9841.
[34] M. C. Hsu, I. C. Leu, Y. M. Sun and M. H. Hon, J. Cryst. Growth, 2005, 285, 642–648.
[35] H. J. Kull, Phys. Rep., 1991, 206, 197–325.
[36] Z. Yue, C. H. Woo and W. Biao, J. Phys.: Condens. Matter, 2008, 20, 135216.
[37] G. Caruntu, A. Yourdkhani, M. Vopsaroiu and G. Srinivasan, Nanoscale, 2012, 4, 3218–3227.
[38] M. Vopsaroiu, M. Stewart, T. Hegarty, A. Muniz-Piniella, N. McCartney, M. Cain and G. Srinivasan, Meas. Sci. Technol., 2008, 19(4), 045106.
[39] D. Damjanovic, Rep. Prog. Phys., 1998, 61, 1267–1324.